Communications

A Self-Catalyzing Hydrogen-Storage Material**

Jun Yang,* Andrea Sudik, Donald J. Siegel, Devin Halliday, Andrew Drews, Roscoe O. Carter, III, Christopher Wolverton, Gregory J. Lewis, J. W. Adriaan Sachtler, John J. Low, Syed A. Faheem, David A. Lesch, and Vidvuds Ozoliņš

Conventional (e.g. MgH_2) and complex hydrides (e.g. alanates, borohydrides, and amides) are the two primary classes of solid-state hydrogen-storage materials.[1–3] Many of these "high-density" hydrides have the potential to store large amounts of hydrogen by weight (up to 18.5 wt% for $LiBH_4$) and/or volume (up to 112 g L^{-1} for MgH_2), values that are comparable to the hydrogen content of gasoline (15.8 wt%, 112 g L^{-1}). However, all known hydrides are inadequate for mobile storage applications due to one or more of the following limitations: a) unfavorable thermodynamics (they require high temperatures to release hydrogen[4]), b) poor kinetics (low rates of hydrogen release and uptake), c) decomposition pathways involving the release of undesirable by-products (e.g. ammonia), and/or d) an inability to reabsorb hydrogen at modest temperatures and pressures (i.e. "irreversibility").

In spite of these drawbacks, renewed interest in complex hydrides has been stimulated recently by substantial improvements in their kinetics and reversibility[5,6] provided by catalytic doping (e.g. $TiCl_3$-doped $NaAlH_4$),[7,8] and by thermodynamic enhancements achieved through reactive binary mixtures[9] such as $LiNH_2/MgH_2$,[10,11] $LiBH_4/MgH_2$,[12] and $LiNH_2/LiBH_4$.[13,14] These compositions, previously termed "reactive hydride composites",[15] represent the state-of-the-art in hydrogen-storage materials; compared to their constituent compounds, they exhibit improved thermodynamic properties, higher hydrogen purity, and, in some cases, reversibility. The desorption behavior of these previously studied composites is illustrated in Figure 1a. It is evident from the hydrogen desorption profile (top panel) that the composites generally desorb hydrogen at significantly lower temperatures than their individual components. For example, the lowest temperature reaction, which involves a
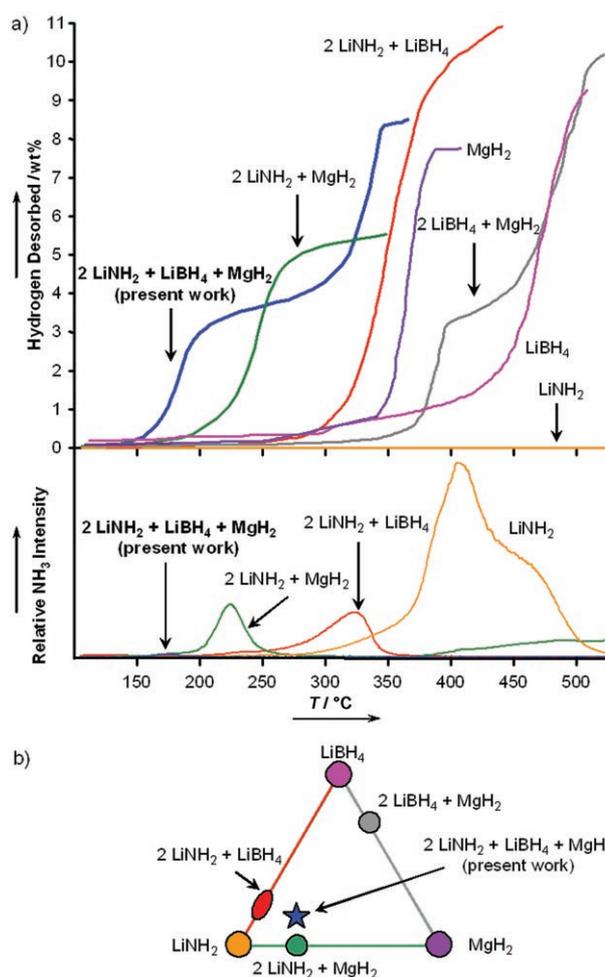
Figure 1. a) Hydrogen (top) and ammonia (bottom) kinetic desorption data as a function of temperature (5 °C min^{-1} to 550 °C) for the ternary composition (blue trace) and its unary and binary constituents. Hydrogen desorption is measured in weight percent (wt%) to 1 bar whereas relative ammonia release is measured as partial pressure (torr) in a flow-through set-up (100 sccm Ar). b) Ternary phase space defined by unary compounds (nodes), $LiBH_4$ (pink), MgH_2 (purple), and $LiNH_2$ (orange) and the binary mixtures (edges), $LiBH_4/MgH_2$ (gray), $MgH_2/LiNH_2$ (green), and $LiNH_2/LiBH_4$ (red). The present ternary composition, which is a 2:1:1 mixture of $LiNH_2$, $LiBH_4$, and MgH_2, and previously investigated binaries, are identified.

[*] Dr. J. Yang, Dr. A. Sudik, Dr. D. J. Siegel, D. Halliday, Dr. A. Drews, Dr. R. O. Carter, III, Dr. C. Wolverton[+]
Ford Motor Company, Research and Advanced Engineering
MD 1170/RIC, P.O. Box 2053, Dearborn, MI 48121 (USA)
Fax: (+1) 313-594-2963
E-mail: jyang27@ford.com

Dr. G. J. Lewis, Dr. J. W. A. Sachtler, Dr. J. J. Low, S. A. Faheem, Dr. D. A. Lesch
UOP LLC
25 East Algonquin Road, Des Plaines, IL 60017-5017 (USA)

Dr. V. Ozoliņš
Department of Materials Science and Engineering
University of California, Los Angeles, CA 90095-1595 (USA)

[+] Current address: Department of Materials Science and Engineering, Northwestern University
2220 Campus Drive, Evanston, IL 60208 (USA)

2:1 mixture of LiNH$_2$ and MgH$_2$, has a desorption temperature more than 100°C lower than that of either MgH$_2$ (approx. 350°C) or LiNH$_2$ (which releases only NH$_3$) alone. Although these binary reactions present significant benefits, they all have well-known disadvantages: a) their lowered desorption temperatures are still too high, b) the reaction involving LiNH$_2$ and LiBH$_4$ is irreversible, c) the nitrogen-containing binaries LiNH$_2$/MgH$_2$ and LiNH$_2$/LiBH$_4$ emit a significant amount of ammonia (a proton-exchange membrane fuel cell (PEM-FC) poison) together with the hydrogen (Figure 1a, bottom panel), and, most significantly, d) hydrogen desorption/uptake in *all* of these binary composites is too slow. Therefore, further improvement in these areas is highly desirable.

Herein we present a strategy for enhancing the properties of binary composites through the creation of a multicomponent composite of three hydride compounds (2LiNH$_2$/LiBH$_4$/MgH$_2$). The improved properties of this system arise almost entirely from a "self-catalyzing" reaction pathway that results in faster kinetics and lower desorption temperatures than for the binary composites and almost complete suppression of ammonia release. The key elements that contribute to the enhanced properties are the incorporation of a low melting temperature ionic liquid (Li$_4$BH$_3$H$_{10}$) and a mechanism for seeding the products of a reversible hydrogen desorption reaction.[16]

The choice of the 2LiNH$_2$/LiBH$_4$/MgH$_2$ stoichiometry is based on several factors: a) the constituent hydrides all possess high gravimetric/volumetric capacities, b) binary mixtures of these hydrides are among the best known hydrogen-storage materials (see Figure 1a, top panel), c) mixtures containing MgH$_2$ are known to suppress ammonia release from nitrogen-containing hydrides such as LiNH$_2$ (Figure 1a, bottom panel), and d) a stable, lightweight compound, namely lithium magnesium boron nitride (LiMgBN$_2$), which contains N, B, and Mg in a 2:1:1 ratio (the same as our stoichiometric composite), is known which could serve as a potential dehydrogenated product phase. The compositional phase space of the ternary composite is shown in the Gibbs triangle in Figure 1b and information regarding the sample synthesis and preparation conditions is given in the Experimental Section.

We begin our discussion of this system by summarizing its principal hydrogen-storage attributes in relation to those of the unary and binary components. Employing a wide range of experimental phase analyses and first-principles evaluation of reaction thermodynamics, we subsequently identify a complex, "cascading" sequence of reactions that explain the observed properties. We conclude with a more detailed discussion of the proposed "self-catalyzing" mechanism.

Lowered desorption temperatures: The measured kinetic desorption behavior (5°C min^{-1}, 1 bar) of the ternary composite is compared with the constituent unary and binary components in the upper panel of Figure 1a. The ternary system rapidly releases hydrogen in a process that begins at 150°C (top panel), which is about 50–200°C lower than the binary composites, thereby indicating significantly improved kinetics and/or thermodynamics. The total capacity of the ternary composite is 8.2 wt%.

Improved hydrogen purity: The composition of the gas released from the ternary composite while heating at 5°C min^{-1} in a flow of 100 sccm argon is plotted in comparison with the binary composites in the lower panel of Figure 1a. The ammonia released by the ternary composite is less than the 100 ppm detection limit of our instrument; the ammonia released from the nitrogen-containing binaries was found to be more than an order of magnitude larger. No other volatile boron- and/or nitrogen-containing by-products were detected throughout the desorption process.

Reversibility: The reversible storage capacity and response to cycling were determined from a series of charge/discharge experiments performed with a Sievert-type PCT apparatus at 160°C and charging (discharging) at 100 (1) bar. The results for five charge/discharge cycles (Figure 2a) show that the as-prepared material rapidly releases approximately 3.0 wt% of hydrogen within 20 minutes. After recharging, the second through fifth
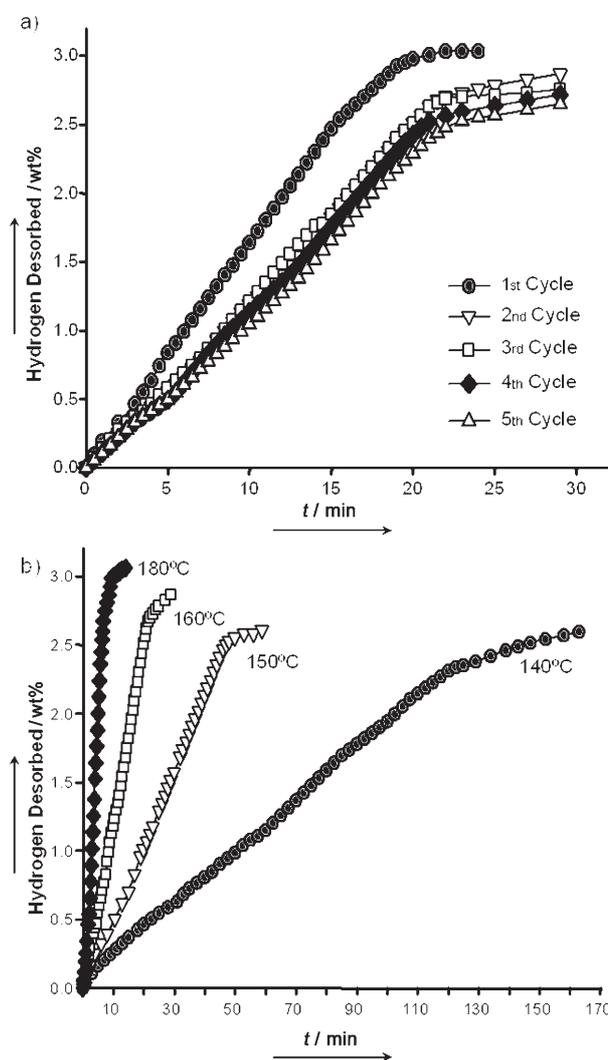
Figure 2. a) Hydrogen desorption kinetics at 160°C and 1 bar over five cycles after subsequent charging (160°C and 100 bar hydrogen). b) Reversible isothermal kinetic hydrogen desorption data (to 1 bar) for the ternary composition based on the second desorption cycle at 140 (●), 150 (▼), 160 (□), and 180°C (♦) versus time.

desorption cycles consistently liberate around 2.8 wt % of hydrogen, a reversible capacity at moderate temperature that is among the best for solid-state hydrogen storage.[5–8]

Kinetics: The reversible isothermal kinetic desorption profiles for the second desorption cycle (to 1 bar) were collected at 140, 150, 160, and 180 °C (Figure 2 b). The ternary composite is capable of desorbing more than 2.5 wt % hydrogen in times ranging from 10 min (180 °C) to 2.5 h (140 °C) in this temperature range. The remaining hydrogen is liberated in a second step at higher temperatures for a total hydrogen capacity of 8.2 wt % (Figure 3). The initial release of hydrogen at both 260 and 320 °C is dramatically accelerated, with 3.2 wt % released within minutes, while the subsequent desorption steps are more influenced by temperature, reaching full desorption after 1.5 and 14 h at 320 and 260 °C, respectively.
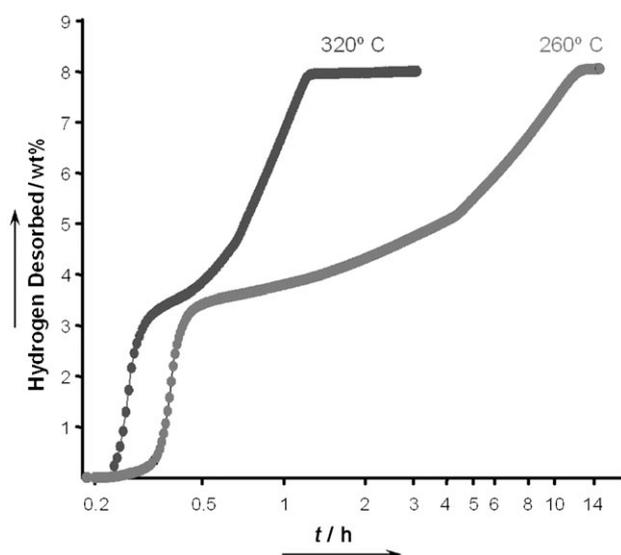
Figure 3. Isothermal kinetic hydrogen desorption to 1 bar for the ternary composition at 260 and 320 °C versus time.

The unique desorption behavior described above strongly suggests that the reaction mechanism(s) of the ternary composite is not a simple superposition of the known binary reactions. To understand its hydrogen-release characteristics, we therefore collected temperature-programmed-desorption mass spectrometry (TPD-MS) data at a constant heating rate and carrier gas flow (5 °C min^{-1}, 100 sccm argon flow; Figure 4 a). Four distinct hydrogen-release events occur (maxima at 180, 190 (shoulder), 310, and 560 °C, respectively), with an initial desorption onset at 110 °C.[17] TPD-MS data were also collected for the cycled/recharged material (See Supporting Information). These data clearly show that the first steep desorption step (at 180 °C) in the as-prepared sample is no longer observed in the recharged sample. Instead, the peak temperature for the recharged sample is now shifted to the shoulder region for the fresh material (approx. 190 °C), thus indicating that the reaction corresponding to the shoulder is reversible, which is consistent with the
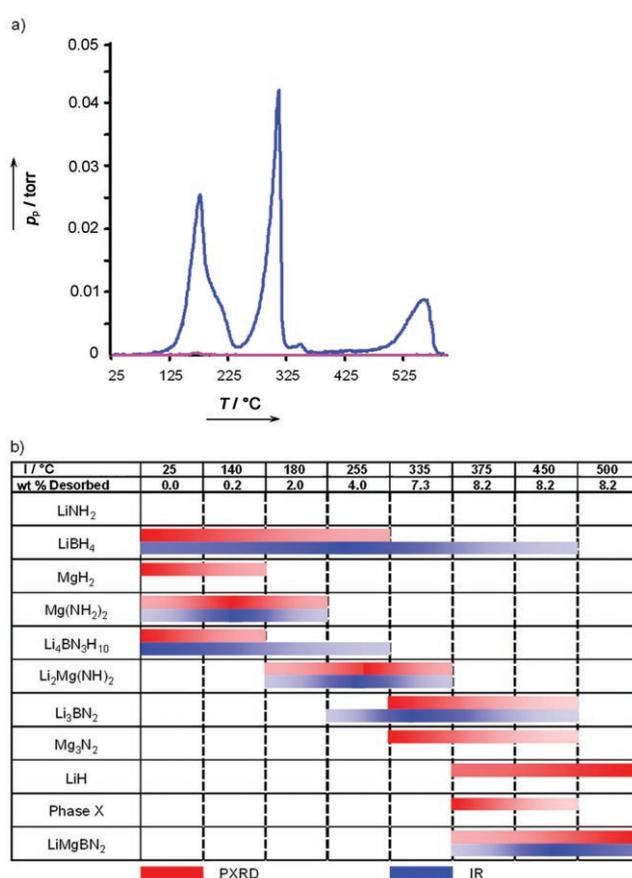
Figure 4. a) TPD-MS data for the ternary composition depicting hydrogen (*m/z* 2, blue) and ammonia (*m/z* 17, pink) as a function of temperature (heating at 5 °C min^{-1} to 575 °C). b) Phase composition as a function of desorbed hydrogen amount (wt %) and temperature (°C) as determined from the static PXRD and IR data.

powder X-ray diffraction (PXRD) and IR spectroscopic analyses (discussed below).

Phase identification: Phase-composition studies were carried out for identically prepared samples, which were desorbed to varying degrees at 1 bar hydrogen by heating at 5 °C min^{-1} in a water displacement apparatus (see Supporting Information) to identify the species involved in the various desorption reactions. Following desorption, each sample was quenched and analyzed by PXRD and IR spectroscopy. The results are summarized in Figure 4 b, and raw data and phase assignments are provided as Supporting Information. The as-prepared sample (ball milling 2 g of LiNH$_2$, LiBH$_4$, and MgH$_2$ in a 2:1:1 ratio for 5 h) contains two new species (Mg(NH$_2$)$_2$ and Li$_4$BN$_3$H$_{10}$) and no residual LiNH$_2$, which is indicative of milling-induced transformations. Residual MgH$_2$ and LiBH$_4$ starting materials are also present. Growth of Mg(NH$_2$)$_2$ and (weakly crystalline) LiH is detected upon initial heating to 140 °C before any appreciable amount of hydrogen is released. At the same time, the diffraction peaks for Li$_4$BN$_3$H$_{10}$ disappear. As the characteristic symmetric and asymmetric amide N−H IR frequencies (observed: 3301 and 3242 cm^{-1}; literature:[18] 3303 and 3243 cm^{-1}) persist, we conclude that Li$_4$BN$_3$H$_{10}$ has melted. Further heating to 180 °C results in the release of 2.0 wt % hydrogen (first low

temperature event in Figure 4a) and the formation of $Li_2Mg(NH)_2$, based on its three characteristic peaks at 30.7°, 51.3°, and 60.9° in the PXRD pattern[19] and the signature N—H stretch in the IR spectrum (observed: 3178 cm^{-1}; literature:[20] 3187 cm^{-1}). This phase continues to grow in intensity until 255°C, at which point 4.0 wt% H_2 has desorbed. At this stage, MgH_2 and $Mg(NH_2)_2$ have been completely consumed while $Li_4BN_3H_{10}$ is significantly depleted.

The second major hydrogen releasing event occurs between 255 and 375°C and corresponds to a total of 8.2 wt% desorbed hydrogen. $Li_2Mg(NH)_2$ and $LiBH_4$ are consumed during this stage and Mg_3N_2 and Li_3BN_2 are formed. Trace amounts of LiH and an unknown phase (denoted as "Phase X") are also detected by PXRD.[21] Further heating to 500°C does not produce additional hydrogen but rather an observed phase transformation consistent with the consumption of Li_3BN_2, Mg_3N_2, and $LiBH_4$ and the production of LiH and $LiMgBN_2$.[22] The final hydrogen releasing step (> 500°C) is attributed to decomposition of LiH (third major event in Figure 4a).

Variable-temperature in situ PXRD was used to validate the above phase assignments and to provide phase transformation information (see the Supporting Information for instrument set-up and data collection protocol). Figure 5a shows the raw PXRD data as a function of temperature (25–450°C) and Figure 5b shows the two-dimensional contour plot. The phase assemblage as a function of temperature is shown in Figure 5c. The data reveal that the sequence and relative phase contributions are identical to those observed by static PXRD, thereby confirming the proposed reaction sequence. Furthermore, the in situ data reveal that the $Li_4BN_3H_{10}$ and MgH_2 phases disappear rapidly (by 100 and 150°C, respectively) during initial heating of the as-prepared material and prior to any hydrogen release. The observed melting of $Li_4BN_3H_{10}$ at 100°C occurs at a significantly lower temperature than previously reported (150°C).[23] This low temperature melt may serve as an effective mass transfer medium or homogenizing agent and aid in the distribution of $Li_2Mg(NH)_2$ (produced in the first desorption step reaction between $Li_4BN_3H_{10}$ and MgH_2), which would in turn serve as $Li_2Mg(NH)_2$ nucleation seeds for a second step reaction

between $Mg(NH_2)_2$ and LiH. The presence of the ionic liquid may therefore positively influence the desorption kinetics of the initial hydrogen release reactions.

Reaction pathway: A set of proposed reactions are summarized in Figure 6. Our assignment of reactions takes into account the observed and theoretical hydrogen capacity for each step, the reversible amount of stored hydrogen, and the phase compositions (obtained from both quenched/static and in situ PXRD and IR spectroscopy). A reaction scheme flowchart is included in the Supporting Information. The TPD-MS curve from Figure 4a is incorporated to indicate the temperature region under which each reaction occurs. The reaction enthalpies (ΔH_{calcd}) and free energies (ΔG_{calcd}) at 300 K obtained by density functional theory calculations are also included in this table. The fact that all the calculated free energies are negative suggests that the proposed reactions are thermodynamically reasonable. (The activation energies for reactions (2) and (4) are given as Supporting Information.)
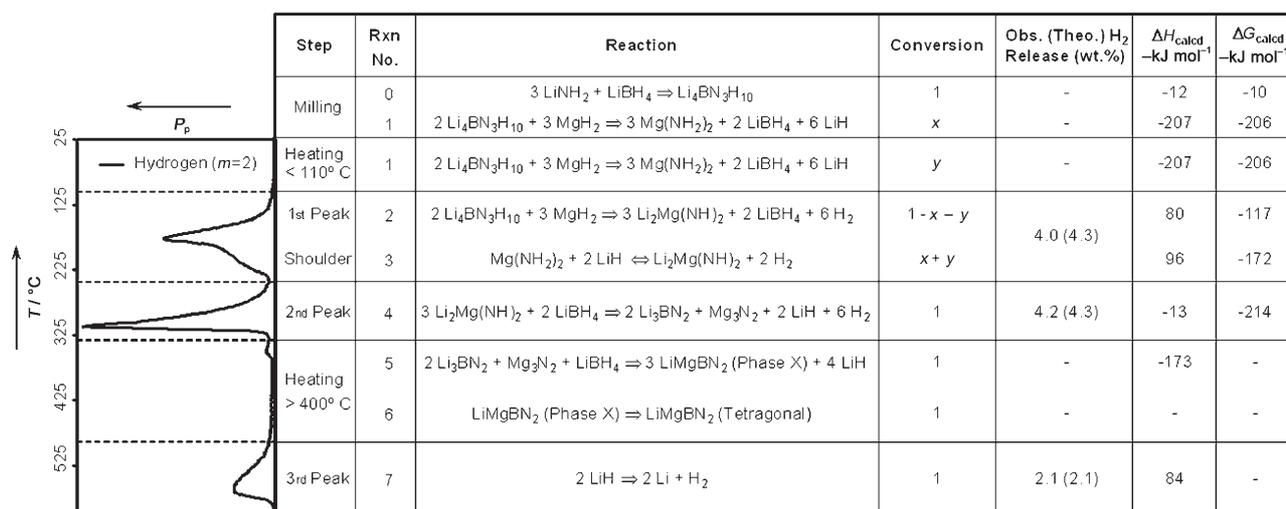
During sample preparation, the starting materials $LiNH_2$ and $LiBH_4$ react to form $Li_4BN_3H_{10}$.[13] Partial reaction of this quaternary phase with a portion of MgH_2 then yields a small amount of $Mg(NH_2)_2$. As both reactions are exothermic (based on DFT calculations), it is likely that they occur under ball milling or upon moderate heating. After milling, the phases present include $Li_4BN_3H_{10}$, $LiBH_4$, MgH_2, $Mg(NH_2)_2$, and LiH. Upon subsequent heating, but before the onset of hydrogen release, production of $Mg(NH_2)_2$ continues according to reaction (1).

$$2\,Li_4BN_3H_{10} + 3\,MgH_2 \rightarrow 3\,Mg(NH_2)_2 + 2\,LiBH_4 + 6\,LiH \qquad (1)$$

Self-catalyzing mechanism: As the temperature reaches 100°C, $Li_4BN_3H_{10}$ melts and reacts with MgH_2 to form $Li_2Mg(NH)_2$ and $LiBH_4$ and releases H_2 at the first low temperature desorption peak [reaction (2)]. This reaction only occurs during desorption of the as-prepared material and not in subsequent cycles (see Supporting Information). More importantly, reaction (2) serves to directly catalyze the subsequent reversible reaction between $Mg(NH_2)_2$ and LiH that occurs at the shoulder region (approx. 190–230°C) [reaction (3)].
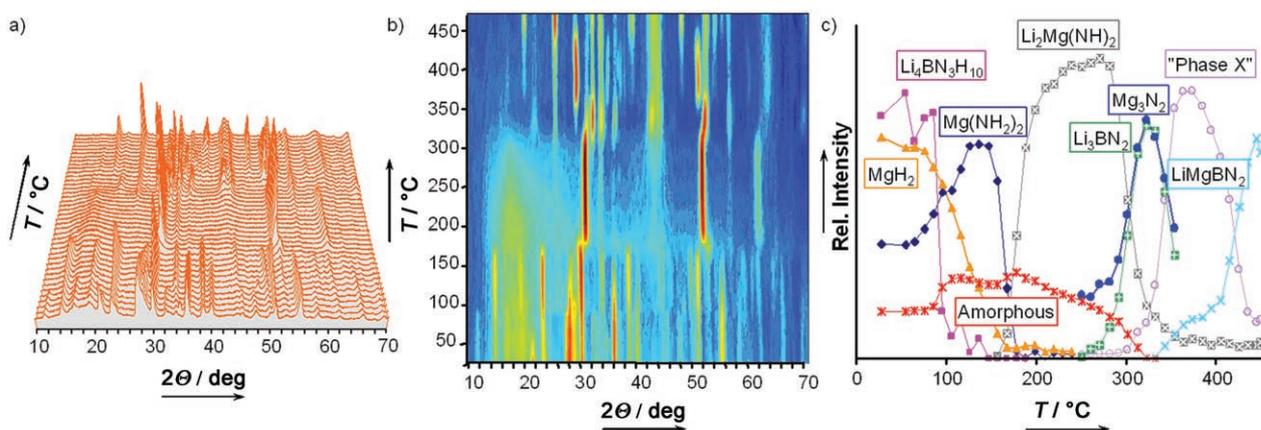
Figure 5. a) Raw PXRD data for the ternary composition as a function of temperature (25–450°C). b) The corresponding two-dimensional contour plot derived from the raw patterns in (a). c) Plot of the relative amounts of individual phases as a function of temperature.

Step	Rxn No.	Reaction	Conversion	Obs. (Theo.) H₂ Release (wt.%)	ΔH_{calcd} –kJ mol⁻¹	ΔG_{calcd} –kJ mol⁻¹
Milling	0	$3\,LiNH_2 + LiBH_4 \Rightarrow Li_4BN_3H_{10}$	1	-	-12	-10
Milling	1	$2\,Li_4BN_3H_{10} + 3\,MgH_2 \Rightarrow 3\,Mg(NH_2)_2 + 2\,LiBH_4 + 6\,LiH$	x	-	-207	-206
Heating < 110° C	1	$2\,Li_4BN_3H_{10} + 3\,MgH_2 \Rightarrow 3\,Mg(NH_2)_2 + 2\,LiBH_4 + 6\,LiH$	y	-	-207	-206
1st Peak	2	$2\,Li_4BN_3H_{10} + 3\,MgH_2 \Rightarrow 3\,Li_2Mg(NH)_2 + 2\,LiBH_4 + 6\,H_2$	$1-x-y$	4.0 (4.3)	80	-117
Shoulder	3	$Mg(NH_2)_2 + 2\,LiH \Leftrightarrow Li_2Mg(NH)_2 + 2\,H_2$	$x+y$		96	-172
2nd Peak	4	$3\,Li_2Mg(NH)_2 + 2\,LiBH_4 \Rightarrow 2\,Li_3BN_2 + Mg_3N_2 + 2\,LiH + 6\,H_2$	1	4.2 (4.3)	-13	-214
Heating > 400° C	5	$2\,Li_3BN_2 + Mg_3N_2 + LiBH_4 \Rightarrow 3\,LiMgBN_2\ (Phase\ X) + 4\,LiH$	1	-	-173	-
Heating > 400° C	6	$LiMgBN_2\ (Phase\ X) \Rightarrow LiMgBN_2\ (Tetragonal)$	1	-	-	-
3rd Peak	7	$2\,LiH \Rightarrow 2\,Li + H_2$	1	2.1 (2.1)	84	-

(TPD-MS curve on left axis: T / °C from 25 to 525; Hydrogen (m=2); P_p)

Figure 6. Proposed reaction pathway for the ternary composite, including the observed/theoretical hydrogen capacity, reaction enthalpy (ΔH), free energy (ΔG) (both in kJ mol⁻¹ for products at 300 K), and the corresponding temperature range (coupled to the TPD-MS curve). The reaction numbers in this figure correspond to those used in the text.

$$2\,Li_4BN_3H_{10} + 3\,MgH_2 \rightarrow 3\,Li_2Mg(NH)_2 + 2\,LiBH_4 + 6\,H_2 \qquad (2)$$

$$Mg(NH_2)_2 + 2\,LiH \rightarrow Li_2Mg(NH)_2 + 2\,H_2 \qquad (3)$$
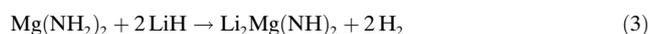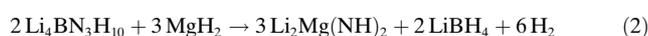
We refer to the ternary composite as "self-catalyzed" in the sense that one reaction [reaction (2)] pre-forms the product nuclei ($Li_2Mg(NH)_2$) for the subsequent reaction [reaction (3)], which results in an enhancement of the overall kinetic properties. A separate study has confirmed the beneficial effects of product seeding in improving the desorption kinetics of the $Mg(NH_2)_2$/LiH system.[24]

It should be emphasized that the thermodynamics of the binary reaction between $Mg(NH_2)_2$ and LiH [reaction (3)] indicate that it should proceed at a lower temperature than observed. Our results suggest a new rational route by which the kinetic properties of existing hydrogen-desorption reactions can be enhanced, namely by coupled self-catalyzing reactions.

Higher-temperature reactions: As the temperature is increased further, $Li_2Mg(NH)_2$ reacts with $LiBH_4$ to form Li_3BN_2, Mg_3N_2, and hydrogen (found: 4.2 wt %; calcd: 4.3 wt %), which corresponds to the second peak [reaction (4)]. This explains why the reversibility in this ternary system is sensitive to desorption temperature and desorbed hydrogen extent. When the sample is heated to above 350 °C, Li_3BN_2, Mg_3N_2, and the remaining $LiBH_4$ react to form "Phase X" and tetragonal $LiMgBN_2$. On additional heating (to around 450 °C), "Phase X" is transformed completely into tetragonal $LiMgBN_2$.[22] Finally, LiH decomposes in the last high-temperature hydrogen releasing step and liberates an additional 2.1 wt % hydrogen (calcd: 2.1 wt %).

$$3\,Li_2Mg(NH)_2 + 2\,LiBH_4 \rightarrow 2\,Li_3BN_2 + Mg_3N_2 + 2\,LiH + 6\,H_2 \qquad (4)$$

In conclusion, our study of the ternary $LiBH_4$/2 $LiNH_2$/MgH_2 composite has led to the discovery of a new "self-catalyzing" strategy for enhancing the kinetics of hydrogen storage in complex hydride composites. We have demonstrated through a wide-ranging experimental and first-principle computational analysis that this self-catalyzing mechanism arises from a set of coupled, ancillary reactions that yield both a homogenizing ionic liquid phase and product nuclei for a subsequent reversible hydrogen-storage reaction. These effects combine to yield enhanced low-temperature desorption kinetics and a significant reduction in ammonia liberation relative to the state-of-the-art binary constituent composites. The strategy of utilizing built-in, ancillary reactions to catalyze a primary hydrogen-storage reaction suggests prospective routes for advancing existing and future storage materials.

Experimental Section

Sample Preparation: $LiNH_2$ (95 % purity, Sigma-Aldrich), MgH_2 (95 % purity, Gelest), and $LiBH_4$ (95 % purity, Sigma-Aldrich) were used as received. All sample handling was performed in an MBraun Labmaster 130 glove box maintained under argon with less than 0.1 ppm O_2 and H_2O vapor. The binary composites 2 $LiNH_2$/$LiBH_4$, 2 $LiNH_2$/MgH_2, and 2 $LiBH_4$/MgH_2 were prepared according to literature protocols.[10,12,13] For the ternary composite, two grams of $LiNH_2$, $LiBH_4$, and MgH_2 in a 2:1:1 molar ratio was loaded into a milling vial containing three stainless steel balls weighing 8.4 g each. Mechanical milling was carried out using a Spex 8000 high-energy mixer/mill for 1–20 h.

Characterization and Property Evaluation: All methods relating to sample characterization and property evaluation, including powder X-ray diffraction (PXRD), IR spectroscopy, kinetic hydrogen desorption/absorption studies (PCT, TPD-MS, and WDD), density functional theory (DFT) calculations, and activation energy calculations are described in detail in the Supporting Information.

[1] P. Dantzer, *Hydrogen in Metals III: Topics in Applied Physics*, Springer, Berlin, **1997**.

[2] W. Grochala, P. P. Edwards, *Chem. Rev.* **2004**, *104*, 1283–1315.

[3] F. Schüth, B. Bodganović, M. Felderhoff, *Chem. Commun.* **2004**, 2249–2258.

[4] High desorption temperatures may also be a consequence of slow kinetics.

[5] B. Bogdanović, M. Schwickardi, *J. Alloys Compd.* **1997**, *253–254*, 1–9.

[6] A. Züttel, P. Wegner, S. Rentsch, P. Sudan, P. Mauron, C. Emmenegger, *J. Power Sources* **2003**, *118*, 1–7.

[7] D. Sun, S. Srinivasan, T. Kiyobayashi, N. Kuriyama, C. M. Jensen, *J. Phys. Chem. B* **2003**, *107*, 10176–10179.

[8] T. Wang, J. Wang, A. D. Ebner, J. A. Ritter, *J. Alloys Compd.* **2007**, DOI: 10.1016/j.jallcom.2006.10.072.

[9] P. Chen, Z. Xiong, J. Luo, J. Lin, K. Tan, *Nature* **2002**, *420*, 302–304.

[10] W. Luo, *J. Alloys Compd.* **2004**, *381*, 284–287.

[11] H. Y. Leng, T. Ichikawa, S. Isobe, S. Hino, N. Hanada, H. Fujii, *J. Phys. Chem. B* **2004**, *108*, 8763–8765.

[12] J. Vajo, S. Skeith, *J. Phys. Chem. B* **2005**, *109*, 3719–3722.

[13] F. E. Pinkerton, G. P. Meisner, M. Meyer, M. Balogh, M. Kundrat, *J. Phys. Chem. B* **2005**, *109*, 6–8.

[14] M. Aoki, K. Miwa, T. Noritake, G. Kitahara, Y. Nakamori, S. Orimo, S. Towata, *Appl. Phys. A* **2005**, *80*, 1409–1413.

[15] M. Dornheim, S. Doppiu, G. Barkhordarian, U. Boesenberg, T. Klassen, O. Gutfleisch, R. Bormann, *Scr. Mater.* **2007**, *56*, 841–846.

[16] Seeding refers to a process by which a small amount of reaction product is added to a chemical reaction in order to increase the nucleation rate of the product phase. Since nucleation can be a rate-limiting process, seeding can yield increased reaction rates.

[17] The difference in onset temperature between the TPD-MS data (110°C) and the kinetic desorption data from Figure 1a (150°C) can be attributed to the pressure difference during data acquisition (100 sccm Ar flow for TPD-MS versus static 1 bar conditions for kinetic desorption experiments).

[18] Y. Filinchuk, K. Yvon, G. Meisner, F. E. Pinkerton, M. Balogh, *Inorg. Chem.* **2006**, *45*, 1433–1435.

[19] Z. Xiong, G. Wu, J. Hu, P. Chen, *Adv. Mater.* **2004**, *16*, 1522–1525.

[20] P. Chen, Z. Xiong, L. Yang, G. Wu, W. Luo, *J. Phys. Chem. B* **2006**, *110*, 14221–14225.

[21] Structural investigations on "Phase X" are on-going although, based on current data, it is thought to be a polymorph of LiMgBN₂.

[22] U. Herterich, J. Curda, K. Peters, M. Somer, H. G. von Schnering, *Z. Kristallogr.* **1994**, *209*, 617.

[23] G. P. Meisner, M. Scullin, M. Balogh, F. E. Pinkerton, M. Meyer, *J. Phys. Chem. B* **2006**, *110*, 4186–4192.

[24] A. Sudik, J. Yang, D. Halliday, C. Wolverton, *J. Phys. Chem. C* **2007**, *111*, 6568–6573.